An EXAFS study of the structure of the metal–support interface in highly dispersed Rh/Al_2O_3 catalysts

J. B. A. D. van Zon, D. C. Koningsberger,[a] H. F. J. van't Blik, and D. E. Sayers[b]
Laboratory for Inorganic Chemistry and Catalysis, Eindhoven University of Technology, P. O. Box 513, 5600 MB Eindhoven, The Netherlands

(Received 26 June 1984; accepted 1 March 1985)

Four highly dispersed and fully reduced rhodium on alumina catalysts with different particle sizes in the range 6–12 Å were investigated with the EXAFS technique in order to derive information about the structure of the metal–support interface. This information can only be obtained when the signal-to-noise ratio of the experimental EXAFS data is high enough and accurate reference compounds and a modified way of data analysis are used. With the aid of phase and amplitude corrected Fourier transforms it was possible to detect a small additional signal which could be ascribed to a Rh–O bond. Since the catalysts were fully reduced and since the intensity of the small signal increased with decreasing particle size, the oxygen neighbor was assigned to be originated from the metal–support interface. From the intensity of the Rh–O bond it was estimated that, on the average, each interfacial rhodium atom is surrounded by 2–3 oxygen ions of the support. The detected Rh–O bond has a coordination distance of 2.7 Å which is about 0.6 Å larger than the first coordination distance in Rh_2O_3 (2.05 Å). The coordination distance of 2.7 Å can be explained by assuming an interaction between metallic rhodium (atomic radius 1.34 Å) and ionic oxygen belonging to the support (ionic radius 1.4 Å). This would possibly imply an ion-induced dipole bonding between the metal particle and the support.

I. INTRODUCTION

Supported metal catalysts are widely used in the chemical and petroleum industry. Such catalysts consist of small metal particles which are dispersed onto an oxidic support, such as Al_2O_3, SiO_2, TiO_2, or MgO. The shape (two or three dimensional), the size, and the composition of the supported metal particles and their interaction with the support surface layer are important subjects with respect to catalytic properties such as selectivity, activity, and stability. Particle sizes are normally smaller than 20 Å and therefore difficult to study. One suitable technique to study these small particles is the EXAFS (extended x-ray absorption fine structure) technique[1–4] since it can be applied to systems lacking long range order. Because EXAFS can determine the local structure around a specific type of atom, it is not only possible to gain information about the metal atoms surrounding a metal atom but also about oxygen ions surrounding this metal atom. Thus it has to be possible to gain information about the interface between the small metal crystallite and the oxidic support. The detectability of the coordination of interfacial metal atoms by oxygen ions in the surface of the support has been discussed in the recent literature.[4–9] Since all metal atoms in the catalyst contribute to the EXAFS signal, the ratio between the amplitude of the EXAFS signal arising from the metal–support interface and the amplitude of the EXAFS signal, originating from the metal–metal bonds in the crystallite, will be low. Therefore, the coordination of interfacial metal atoms with support oxygen ions can only reasonably be detected in highly dispersed catalysts, containing very small metal particles with a relatively large metal–support interface.

In this paper we will present an EXAFS study on highly dispersed rhodium catalysts which are supported on alumina. Measurements were carried out on four catalysts with different particle sizes in the range from 6 to 12 Å diameter. After reduction the bonding between the metal crystallite and the support was studied as a function of particle size. In addition, the catalyst with the highest dispersion was also measured after impregnation and drying, to study the bonding between the precursor ($RhCl_3$) and the support.

Since the amplitude of the EXAFS signal arising from the metal–support interface is very small, accurate data for EXAFS phase and amplitude functions are required both for the catalyst samples and the three reference compounds [rhodium metal foil, rhodium (III) oxide, and rhodium (III) chloride]. Due to the interference between the signal arising from the metal–support interface with the signal arising from the metal–metal bonds in the crystallite, a modification of the usual data analysis involving phase and amplitude corrected Fourier transforms has been developed. The imaginary part of the Fourier transform has been used to identify the different types of scattering atoms which contribute to the EXAFS spectrum.

II. EXPERIMENTAL

For this study different $Rh/\gamma\text{-}Al_2O_3$ catalysts were prepared by changing the metal loading and the reduction temperature. This resulted in four catalysts with different average particle sizes in the range 6–12 Å. The weight percentages were: 0.57 wt. % (A), 0.47 wt. % (B), 1.04 wt. % (C), and 2.00 wt. % (D). The rhodium content of the catalysts was determined colorimetrically. All catalysts were prepared by incipient wetting of $\gamma\text{-}Al_2O_3$ with an aqueous solution of $RhCl_3 \cdot 3H_2O$ (39 wt. %, Drijfhout). The support $\gamma\text{-}Al_2O_3$ which was used for catalyst A and D (BET area of 150 $m^2\ g^{-1}$, pore volume of 0.65 $cm^3\ g^{-1}$) was obtained by

[a] To whom correspondence should be addressed.
[b] Department of Physics, North Carolina State University, Raleigh, NC 27650.

 0021-9606/85/125742-13$02.10

TABLE I. Details of catalyst preparation and treatment. Results of hydrogen chemisorption measurements.

Catalyst	Weight %	Drying T(k)/t(hr)	Prereduction T(k)/t(hr)	Reduction T(k)/t(hr)	H/Rh
A	0.57	393/20	-	573/1	1.7
B	0.47	300/14 + 393/16	773/1	773/1	1.7
C	1.04	300/14 + 393/16	773/1	773/1	1.65
D	2.00	363/3	573/6.5	573/1	1.2

heating boehmite (supplied by Martinswerk GmbH) at 873 K. The support, which was used for catalysts B and C, was a γ-Al_2O_3 of Ketjen (000-1.5E, BET area of 290 $m^2\ g^{-1}$, pore volume of 0.65 $cm^3\ g^{-1}$). After impregnation, catalyst A was dried in air at 393 K for 20 h to remove the adsorbed water, catalysts B and C were dried overnight at room temperature and subsequently for 16 h at 393 K, while catalyst D was dried at 373 K for 3 h. After drying, catalyst A was stored for further use. Catalysts B and C were directly reduced at 773 K (heating rate 5 K min^{-1}) for 1 h in flowing hydrogen (researchgrade, Hoekloos), cooled down to 300 K, and passivated (controlled oxidation at room temperature). Catalyst D was directly reduced at 573 K for 6.5 h, again followed by a passivation. Details of the preparation procedure are compiled in Table I.

After reduction at 573 K hydrogen chemisorption measurements were performed in a conventional glass system at 298 K. They resulted in H/Rh values (the total amount of chemisorbed H atoms per total amount of rhodium) which are presented in Table I. Temperature programmed reduction (TPR) studies confirmed that the reduction of the catalysts was complete. Further detailed information about chemisorption and TPR is extensively reported.[3,10] The H/Rh values and also the TPR results indicate that the systems contain small metal crystallites and indeed are highly dispersed.

The x-ray absorption spectra of the catalysts performed on the *K*-edge of rhodium (23219.8 eV) were measured on beam line I-5 at the Stanford Synchrotron Radiation Laboratory (SSRL), operating at 3 GeV beam energy and 40–80 mA beam current. The rhodium *K*-edge calibrations, which are used for the EXAFS experiments, carried out in this work do not give *K*-edge energy values with an accuracy better than 4 eV. The catalysts were made as thin pressed self-supporting wafers (thickness in accordance with an optimal signal-to-noise ratio) and were mounted in an EXAFS cell, designed for *in situ* treatments and measurements.[11] Catalyst A was reduced *in situ* at 573 K, the passivated catalysts B and C were rereduced at 773 K, and catalyst D was rereduced at 573 K, all for 1 h under 100 kPa of flowing hydrogen. The EXAFS spectra were recorded in a hydrogen atmosphere both at liquid nitrogen and room temperature.

The data analysis was carried out with experimentally determined phase shift functions and backscattering amplitudes instead of theoretical values. To extract the necessary functions, three reference compounds with known crystal structures were measured: (i) rhodium metal foil with a thickness of 20 μm, (ii) powdered $RhCl_3$, mixed with alumina, (iii) powdered Rh_2O_3, made by oxidizing rhodium metal for 3 days at 1073 K, mixed with alumina. The rhodium (III) oxide structure was checked with x-ray diffraction.

III. DATA ANALYSIS

The EXAFS function $\mu(k)$ is defined as $\mu(k) = (\mu - \mu_0)/\mu_0$, where μ is the measured x-ray absorption coefficient and μ_0 is the absorption coefficient of the isolated atom. The wave vector of the outgoing photoelectron k is related to the kinetic energy of the electron, E_{kin}, by the equation $E_{kin} = \hbar^2 k^2/2m$ ($E_{kin} = h\nu - E_0$), $h\nu$ the photon energy, E_0 the binding energy of the electron. The difference $\mu - \mu_0$ represents the EXAFS oscillations, subtracted from the background, while the division by μ_0, which is proportional to the number of absorbing atoms, normalizes the EXAFS oscillations to a per atom basis.

To remove the EXAFS oscillations from the measured absorption coefficient μ, we use a cubic spline background subtraction.[12] The advantage of the cubic spline procedure over a common polynomial subtraction is that one is able to separate small variations in the background from the EXAFS signals. The calculation of the background is controlled by a smooth parameter which is chosen in such a way that the remaining EXAFS oscillations which are present in the derivative of the background, are just visible. This criterion results in the best separation between the EXAFS oscillations and the background which is very important for small signals.

The EXAFS oscillations are normalized to an EXAFS signal per absorbing atom through division by the height of the absorption edge which is proportional to the total number of absorbing atoms. By making use of empirical phase and amplitude functions, derived from reference compounds, only a step normalization is necessary since the reference compounds are normalized in the same way as the catalysts.

A general equation which relates the important structural parameters to the measured EXAFS oscillations $\chi(k)$ has been given by Stern *et al.*[13–15]:

$$\chi(k) = \sum_j A_j \sin[2kR_j + \varphi_j(k)]. \tag{1}$$

The EXAFS function is a superposition of contributions from different coordination shells where the index j refers to the jth coordination shell. R_j is the average coordination distance between the absorbing atom and the neighbor atoms in the jth coordination shell, $\varphi_j(k)$ the phase shift which the photoelectron undergoes during the outgoing and scattering process. $A_j(k)$ is the amplitude function which is expressed as follows:

$$A_j = \frac{N_j}{kR_j^2} S_0^2(k) f_j(k) e^{-2k^2\sigma_j^2} e^{-2(R_j - \Delta)/\lambda}. \tag{2}$$

N_j is the average number of scatterer atoms in the jth coordination shell, σ_j^2 the mean square deviation about the average coordination distance R_j, caused by thermal motion and/or static disorder. $f_j(k)$ is the backscattering amplitude, charac-

teristic for a particular type of neighboring atom. $S_0^2(k)$ corrects for the relaxation of the absorbing atom and multielectron excitations.[13] λ is the mean free path of the photoelectron, Δ is a correction term ($\Delta \simeq R_1$) in the mean free path concept, because $S_0^2(k)$ and $f(k)$ already account for most of the photoelectron losses in the first coordination shell. Equations (1) and (2) are only valid in the case of a small disorder with a Gaussian pair distribution function.[16–19]

Since the EXAFS function is a superposition of an unknown number of coordination shells, the Fourier transform technique is used to gain information about the individual shells. The Fourier transform of the EXAFS function, $\theta_n(r)$, is generally expressed as

$$\theta_n(r) = \frac{1}{\sqrt{2\pi}} \int_{k\,\min}^{k\,\max} k^n \chi(k) e^{2ikr}\, dk. \tag{3}$$

The function $\chi(k)$ can be weighted by a power of k to equalize the envelope of $\chi(k)$ over the transformation range. Commonly used powers are $n = 1,2,3$, dependent on amplitude variation and signal-to-noise ratio of the measured signal. To minimize truncation errors which are caused by the finite integration range, the limits of integration, k min and k max, are chosen in such a way that these k values coincide with nodes in the function $\chi(k)$. Further minimization of these errors can be obtained by using a window function $W(k)$, such as a cosine shaped Hanning window or a Gaussian window. The function $\theta_n(r)$ will contain peaks whose positions are related to the coordination distances R_j which are present in the measured EXAFS function but these peaks are shifted towards lower R values because of the phase shift $\varphi_j(k)$.[20]

In the next section the various techniques to extract numerical values of the important structural parameters N_j, R_j, and σ_j^2 will be discussed. Which technique is used depends on the structural information which is contained in the catalyst.

When all coordination peaks in the RDF are well separated from each other and when one single peak contains only information of a single absorber–scatterer pair, the shell of interest can be filtered out by performing consecutively a forward and an inverse Fourier transformation. Windows can be used also in this case, but normally we choose the limits of filtering in r space such that they coincide with nodes in the imaginary part of the complex Fourier transform, in analogy with the forward transformation. From the inverse transformation the phase and the amplitude of $\chi(k)$ can be calculated as a discrete function of k. The use of these tabulated functions avoids the need of parametrizing phase and amplitude and thus avoids errors introduced by an inadequate parametrization. The phase and the envelope of the inverse transformed signal will be denoted as $\varphi(k)$ and $A(k)$.

Assuming an energy shift ΔE_0 in the position of the edge of the catalyst with respect to the edge position of the reference compound, the relation between the photoelectron wave vector k and the wave vector of the reference compound k_r will be given in first order by Eq. (4):

$$k_r = \left[k^2 + \frac{2m}{\hbar^2} \Delta E_0\right]^{1/2}. \tag{4}$$

By making use of the phase transferability concept [$\varphi_r(k_r) = \varphi(k)$], between the (metal) catalyst and the (metal) reference compound, correct values for the unknown interatomic distance R and energy shift ΔE_0 can simultaneously be determined from the linear minimization of the function:

$$\sum_k \left[\Phi(k) - 2kR - \varphi_r(k) - \frac{m\Delta E_0}{\hbar^2 k} \frac{\partial \varphi_r}{\partial k_r}\Big|_{k_r = k}\right]^2. \tag{5}$$

The function $\Phi(k)$ [$= 2kR + \varphi(k) + 2n\pi$] is the measured sine argument in the EXAFS function of the catalyst. Equation (5) has been derived to first order in k by a Taylor expansion of $\Phi_r(k_r)$ about $\Phi(k)$ where Eq. (4) has been used to relate k to k_r. The summation extends over all discrete k values for which $\Phi(k)$ and $\Phi_r(k_r)$ are known. The integer n corrects for possible 2π phase shifts between the catalyst and the reference compound. Since the function $\varphi_r(k_r)$ is known from the reference compound, the derivative $\partial\varphi_r/\partial k_r$ can easily be calculated by a computer. This method of determining R and ΔE_0 simultaneously matches the intercept and the slope of the phase shift of the sample with those of the reference compound.

After the determination of R and ΔE_0, the coordination number N and the relative squared disorder parameter $\Delta\sigma^2$ (i.e., the difference between the squares of the disorder parameters of sample and reference compound) can be extracted from the envelope function $A(k)$ using the ratio technique.[20] The quotient of the envelopes $A(k)$ and $A_r(k)$ becomes

$$\ln\left[\frac{A(k)}{A_r(k)}\right] = \ln\left[\frac{NR_r^2}{N_r R^2}\right] - 2k^2(\sigma^2 - \sigma_r^2). \tag{6}$$

Equation (6) is valid under the assumption that S_0^2, f, λ, and Δ are approximately equal for the sample and its reference compound. Equation (6) gives a straight line when it is plotted vs k square. From the intercept of the line the unknown coordination number N can be determined and from the slope of the line the relative disorder can be found. From the shape of the log plot a good impression of the accuracy in the determination of N and $\Delta\sigma^2$ can be obtained. Moreover, the log plot gives a convenient check whether only one type of scatterer is present in the inverse transformed shell.

When the Fourier transform shows an overlap between different coordination shells, other techniques have to be applied. One technique that is frequently used is the technique of fitting in k space. In this technique a multiple shell formula like Eq. (1) is fit to the experimental or inverse transformed EXAFS signal. Such a fitting process is accompanied by a large number of freely adjustable parameters (three to four parameters per shell). We have found that the reliability of the parameters which are obtained by the fitting procedure in k space can be checked by comparing the Fourier transform (the imaginary part as well as the magnitude) of the experimental data with the Fourier transform of the EXAFS function calculated with these parameters. This criterion provides a sensitive check that the right frequency components are used, since it is possible that small differences in k space, not belonging to the fitted coordination distances, are compensated by wrong parameter values. If the various

coordination shells to be fitted are approximately equal in amplitude, the fitting technique is reasonably accurate, but whenever shells with small magnitudes have to be analyzed in the presence of stronger shells, the technique becomes less reliable. Specifically in the case of our catalysts, where a small oxygen contribution may be hidden by a strong metal–metal peak, a different approach of data analysis has to be used.

A normal k^1-weighed Fourier transform of a Rh–Rh EXAFS signal introduces in r space sidelobes on both sides of the peaks. A small contribution to the sidelobes is caused by the finite integration range which cannot start at $k = 0$ $Å^{-1}$. The major part of the sidelobes is due to the nonlinearity in the phase shift function and the low frequency variation in the backscattering amplitude. These low frequency variations increase with increasing atomic number and are important for elements which have an atomic number higher than titanium ($Z = 22$). Sometimes, these sidelobes may have an intensity which is up to 30%–40% of the intensity of the main peak. When peaks due to other shells are close to the main peak, these sidelobes of the main peak significantly interfere with the signal of the other shells. Using standard Fourier transform techniques, it is impossible to separate these peaks by an inverse transformation. By increasing the power of the weight factor k^n in the Fourier transform, the intensities of the sidelobes are reduced. However, this also amplifies the noise at high k values. The most important disadvantage in using higher n values is that the Fourier transform becomes less sensitive to the contributions of low Z scatterers (like oxygen), which have their scattering amplitude primarily at low k values.

A Fourier transformation, which corrects for the nonlinearities in the phase shift function and the variations in the backscattering amplitude, reduces to a transform of a sinelike function with only very small sidelobes due to truncation effects.[21] Such a correction can be done by elimination of $\varphi(k)$ and $f(k)$ in $\chi(k)$ [Eq. (3)], converting it to the form $\chi(k) \cdot \exp[-i\varphi(k)]/f(k)$ before a transformation is carried out. This is possible because normally the functions $\varphi(k)$ and $f(k)$ can be accurately derived from suitable model compounds. This phase and backscattering amplitude corrected Fourier transform will be referred to as FT′. The effect of phase and amplitude correction on the shape of the peak in the radial structure function is shown in Fig. 1. A one shell Rh–Rh EXAFS function is calculated by means of experimental phase and amplitude functions determined from rhodium metal foil. In Fig. 1(a) a standard k^1-weighed Fourier transform is shown. The transformation range was chosen such that truncation effects could be neglected. Clearly visible is the large sidelobe on the left side of the main Rh–Rh coordination peak. A Fourier transform which is only phase corrected is shown in Fig. 1(b). The peak becomes more symmetric with two identical sidelobes, caused by the low frequency amplitude variation. After phase and amplitude correction (giving FT′), one obtains a symmetrical peak without sidelobes [Fig. 1(c)]. Note that the imaginary part of this transform has a simple and symmetric r dependence, peaks at the magnitude of the radial structure function, and is located at the actual coordination distance. Observing the

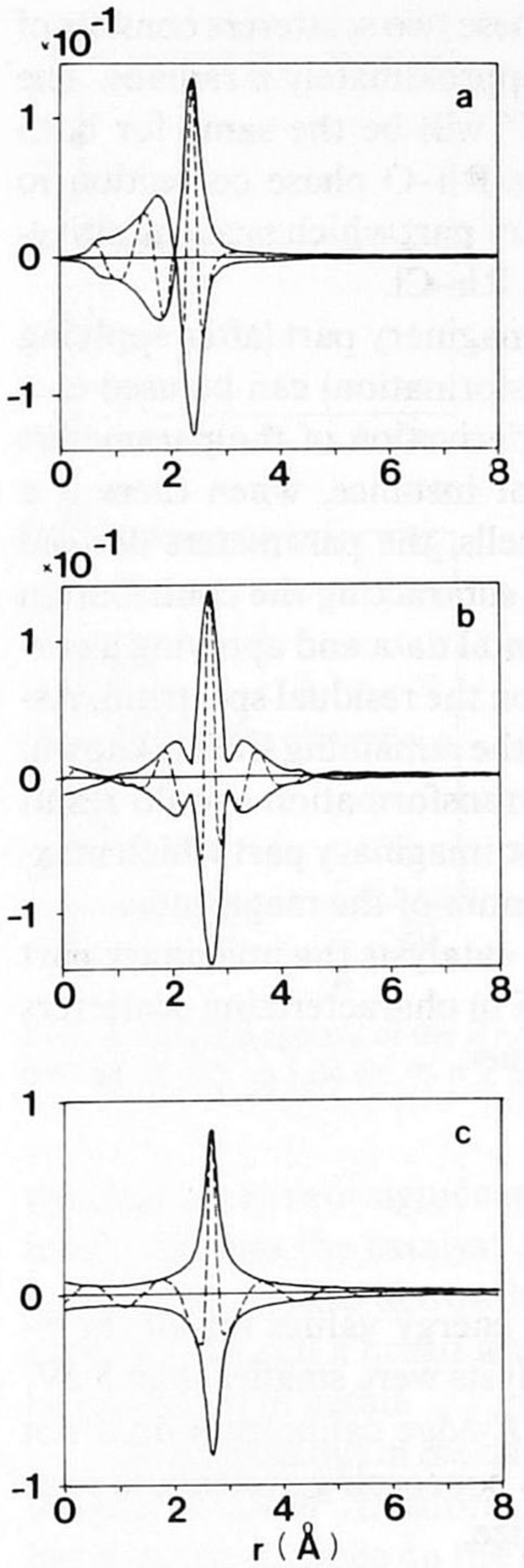

FIG. 1. Imaginary part (dotted line) and magnitude (solid line) of the Fourier transform (k^1-weighed, $\Delta k = 2.68$–24.4 $Å^{-1}$) of a single shell Rh–Rh EXAFS ($N = 6$, $R = 2.687$, $\Delta\sigma^2 = 0.005$): (a) normal, (b) Rh–Rh phase corr., (c) Rh–Rh phase and amplitude corr.

imaginary part together with the magnitude in a corrected Fourier transform has several important advantages with respect to only using the magnitude of a normal Fourier transform:

(i) When the imaginary part of a FT′ which is corrected for the phase and amplitude of a specific absorber–scatterer pair, is asymmetric, it immediately indicates that contributions of other types of atoms are present.

(ii) The imaginary part can give much more information than the absolute part since both phase and amplitude information are contained in it. A peak in the magnitude of the FT does not necessarily correspond with a real interatomic distance. Since the imaginary part consists of high frequency oscillations, two different but nearby coordination distances may cause severe interference patterns which can result in the extinction of one coordination distance and/or the amplification of a feature in the imaginary part which does not correspond with a real coordination distance. Therefore assignments of coordination distances based only upon the magnitude of the FT may result in a wrong interpretation of the spectrum. By studying the shape of the imaginary part of several possible absorber–scatterer pairs under various transform corrections, it is possible to unravel complicated imaginary parts and anticipate interference effects.

(iii) The imaginary part can be used to easily distinguish between possible scatterers. In our catalysts two low-Z elements, O and Cl, can both be present in the EXAFS spec-

trum. The difference between these two scatterers consists of a constant phase difference of approximately π radians. The shape of the magnitude of FT′ will be the same for both elements. However, applying a Rh–O phase correction to the FT will result in an imaginary part which peaks positively for Rh–O and negatively for Rh–Cl.

(iv) The symmetry of the imaginary part (after applying the appropriate corrected transformation) can be used as a mathematical criterion in the derivation of the parameters for that coordination shell. For instance, when there is a strong overlap between two shells, the parameters derived for one shell can be checked by subtracting the contribution of that shell from the experimental data and applying a corrected Fourier transformation on the residual spectrum. Assuming that the type of atom in the remaining shell is known, this second corrected Fourier transformation should result in a single peak with a symmetric imaginary part which maximum coincides with the maximum of the magnitude.

During the analysis of our catalysts the imaginary part of the FT′ was extensively used in characterizing scatterers and determining parameter values.

IV. RESULTS

A. *K*-edges

The differences in *K*-edge energy values for all the γ-Al_2O_3 supported rhodium catalysts were smaller than 5 eV. The accuracy of the rhodium *K*-edge calibration does not permit any definite conclusions concerning systematic edge shifts as a function of particle size.

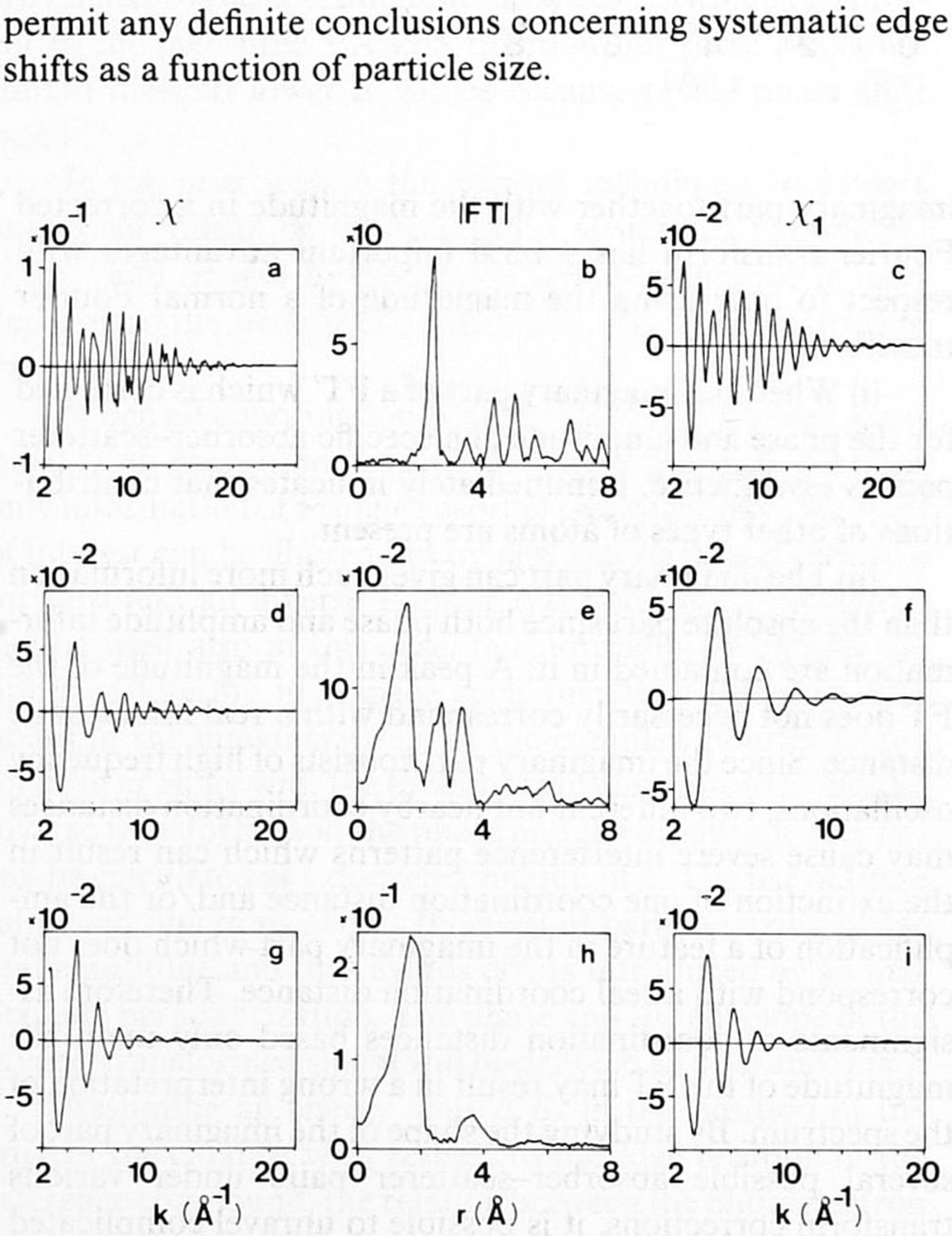

FIG. 2. EXAFS data of the reference compounds. Rhodium foil: (a) $\chi(k)$ (b) FT (k^1-weighed, $\Delta k = 2.68$–24.4 Å^{-1}), (c) χ_1($\Delta R = 1.5$–3.05 Å). Rh_2O_3: (d) $\chi(k)$, (e) FT (k^1-weighed, $\Delta k = 2.7$–18 Å^{-1}), (f) χ_1($\Delta R = 0$–2.05 Å). $RhCl_3$: (g) $\chi(k)$, (h) FT (k^1-weighed, $\Delta k = 2.7$–18 Å^{-1}), (i) χ_1($\Delta R = 0$–2.5 Å).

TABLE II. Crystallographic data and Fourier transformation ranges of reference compounds.

Reference compound	k^n	Δk (Å^{-1})	ΔR (Å)	R_{ref} (Å)	N_{ref}
Rh foil	k^3	2.68-24.4	1.5-3.05	2.687	12
Rh_2O_3	k^1	2.7-18	0-2.05	2.05	6
$RhCl_3$	k^1	2.7-18	0-2.5	2.31	6

B. Reference compounds

Figures 2(a), 2(d) and 2(g) present the EXAFS functions of the three reference compounds rhodium foil, Rh_2O_3, and $RhCl_3$, measured at liquid nitrogen temperatures, while Figs. 2(b), 2(e), and 2(h) show the corresponding radial structure functions. The parameters used for the Fourier transformation are given in Table II. All the data have a very good signal-to-noise ratio, allowing a large transformation range. In the magnitude of the FT for rhodium foil as many as six coordination shells can be seen. This also indicates the high quality of the data. In all cases the first coordination shell is well separated from the other coordination shells, so reliable phase and amplitude functions can be obtained from the inverse transformation. The isolated single shell functions with their envelopes are plotted in Figs. 2(c), 2(f), and 2(i). Care must be taken to use these functions since, due to the finite transformation range, distortions are present at the start and the end of the range. The crystallographic data (N_1, R_1) which were used in the extraction of the experimental phase and amplitude functions, are given in Table II. Since the determined backscattering amplitudes still contain an unknown static and thermal disorder and a damping due to photoelectron losses in the first shell, the values of the disorder parameter reported for the catalysts will be given relative to the reference compound.

C. Rh(0.57 wt. %)/Al_2O_3 catalyst, after impregnation and drying

Before rhodium was reduced to the metallic state, an EXAFS measurement was carried out on an impregnated and dried catalyst in order to gain information about the state of the $RhCl_3$ on the support. Figure 3(a) presents the raw EXAFS data of the impregnated catalyst. The FT of the untreated catalyst [Fig. 3(b)] has been compared with the Fourier transforms of $RhCl_3$ [Fig. 2(h)] and Rh_2O_3 [Fig. 2(e)] to obtain a first impression of the interpretation of the EXAFS spectrum. The first shell coordination distance in the radial structure function of the catalyst is about equal to the first shell distance in the FT of the Rh_2O_3 reference compound, but the magnitude of the Fourier transform of the catalyst differs largely from that of Rh_2O_3. Thus, regarding the amplitude of the transform of the impregnated catalyst, the EXAFS function can not be explained by only oxygen ions as scatterers. Most likely there are contributions from oxygen as well as from chlorine neighbors. To analyze the contributions of each ion, the following method was used. An EXAFS function containing both ions as neighbors was

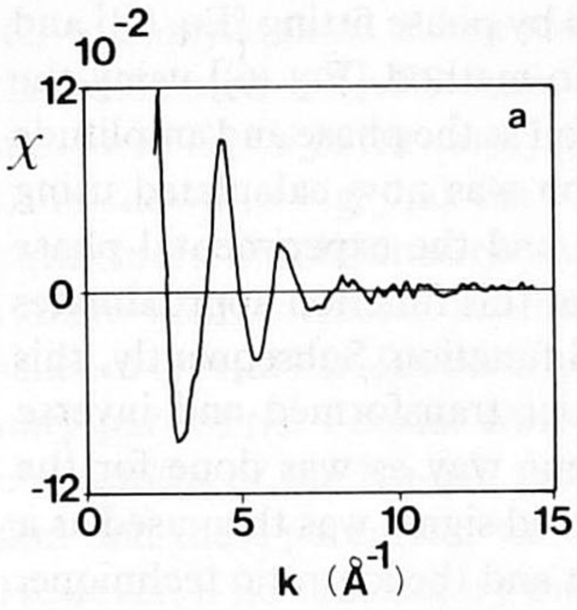

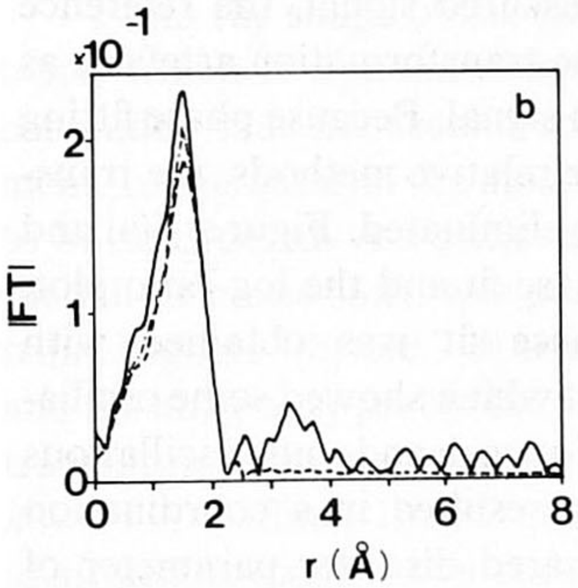

FIG. 3. Impregnated and dried 0.57 wt. % Rh/Al_2O_3 catalyst: (a) EXAFS spectrum, (b) normal Fourier transform (k^1-weighed, $\Delta k = 2.58$–10 Å^{-1}) of experimental data (solid line), of calculated EXAFS: (- - -) ($N_{Rh-O} = 3$, $N_{Rh-Cl} = 3$), (-----) ($N_{Rh-O} = 3.8$, $N_{Rh-Cl} = 3$).

calculated as a function of N_O (number of oxygen scatterers), while keeping N_{Cl} (number of chlorine scatterers) equal to $6\text{-}N_O$. This was done because the rhodium ions in the catalyst have a valence state of 3+ (proven by TPR experiments)[10] and the most likely coordination number of Rh^{3+} ions is six. The mean square deviation between this calculated EXAFS function and the EXAFS function obtained by backtransformation of the main peak in the Fourier transform of the impregnated catalyst can be calculated as a function of N_O. Equal contributions of chlorine and oxygen give the best fit to the experimental results. The Fourier transform of the optimal calculated EXAFS is shown in Fig. 3(b). Some deviations still exist between $R = 0.5$ Å and $R = 2$ Å. Although chemically the sum of the coordination numbers N_O and N_{Cl} cannot exceed 6, the fit can be improved by increasing the oxygen coordination number to about 3.5–4. The Fourier transform of the EXAFS calculated with $N_{Cl} = 3$ and $N_O = 3.8$ is also presented in Fig. 3(b).

In the next section the results of the reduced catalysts will be presented. The full data analysis will be presented for catalyst B. The other catalysts have been analyzed using the same procedure.

D. Catalyst B, Rh(0.47 wt. %)/Al_2O_3, reduced at 773 K

Figure 4(b) shows the EXAFS function of catalyst B, measured at room temperature. The spectrum was Fourier filtered to remove most of the high frequency noise components. Figures 5(a) and 5(b) show the magnitude and the imaginary part of the k^1-weighed Fourier transform from k min $= 3.3$ Å^{-1} to k max $= 12.7$ Å^{-1}. The integration limits are chosen in nodes of the EXAFS function resulting in a integration over an integral number of oscillations. The FT shows the following features: (i) a main peak at approximately 2.4 Å which must unquestionably be assigned to the first shell rhodium–rhodium distance in the metal crystallite, (ii)

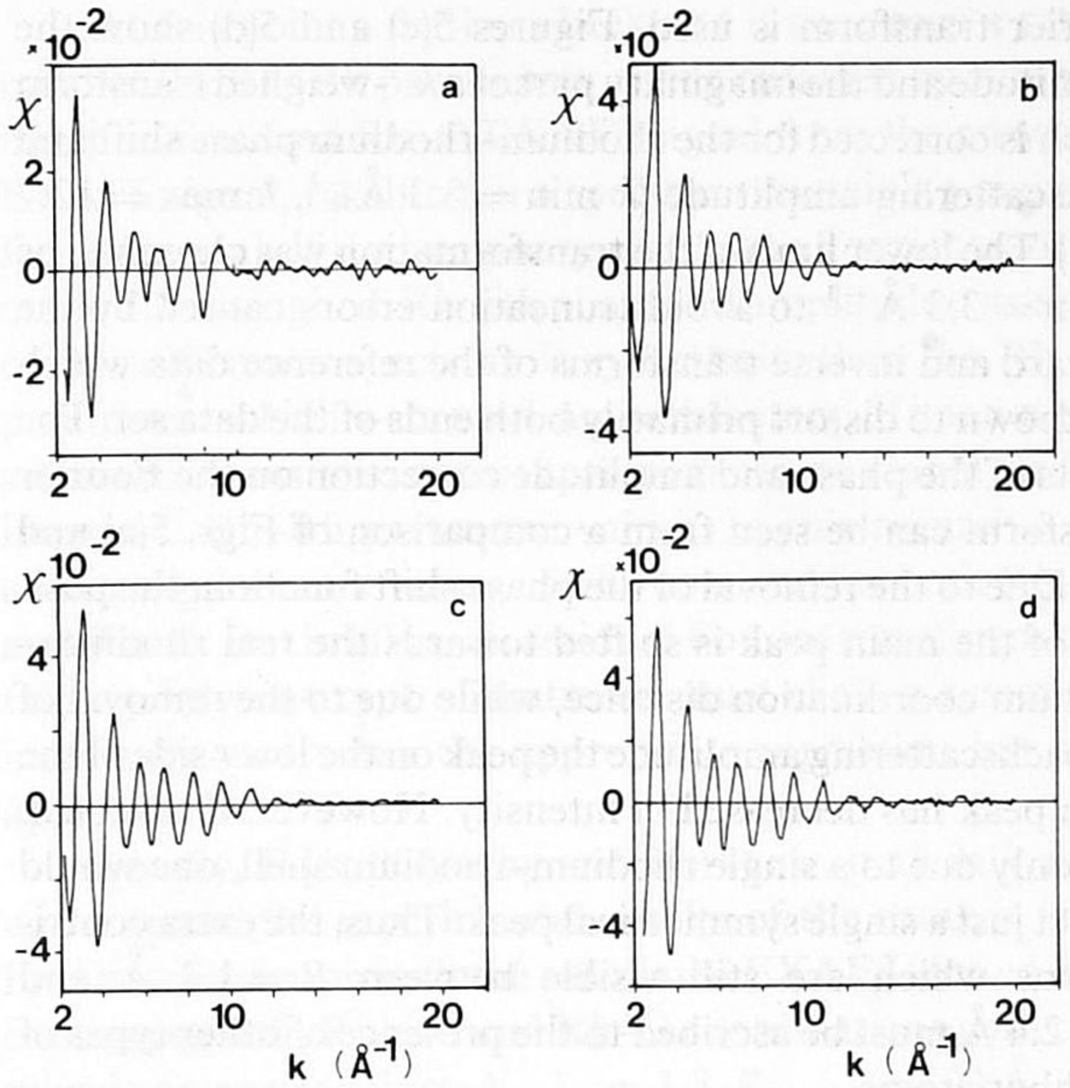

FIG. 4. EXAFS spectra of the Rh/Al_2O_3 catalysts: (a) 0.57 wt. % (A), (b) 0.47 wt. % (B), (c) 1.04 wt. % (C), (d) 2.00 wt. % (D).

the clear absence of significant contributions of higher shells, indicating that the catalyst consists primarily of very small crystallites, as also shown by the hydrogen chemisorption experiments, (iii) a broad feature at low R values which will be examined in detail.

As pointed out in the data analysis section, a normal k^1-weighed Fourier transform of a Rh–Rh EXAFS function has a strong sidelobe on the left side of the main peak. In the present case this sidelobe may drastically interfere with other possible contributions in that region. To reduce or eliminate these sidelobe effects, a phase and amplitude corrected

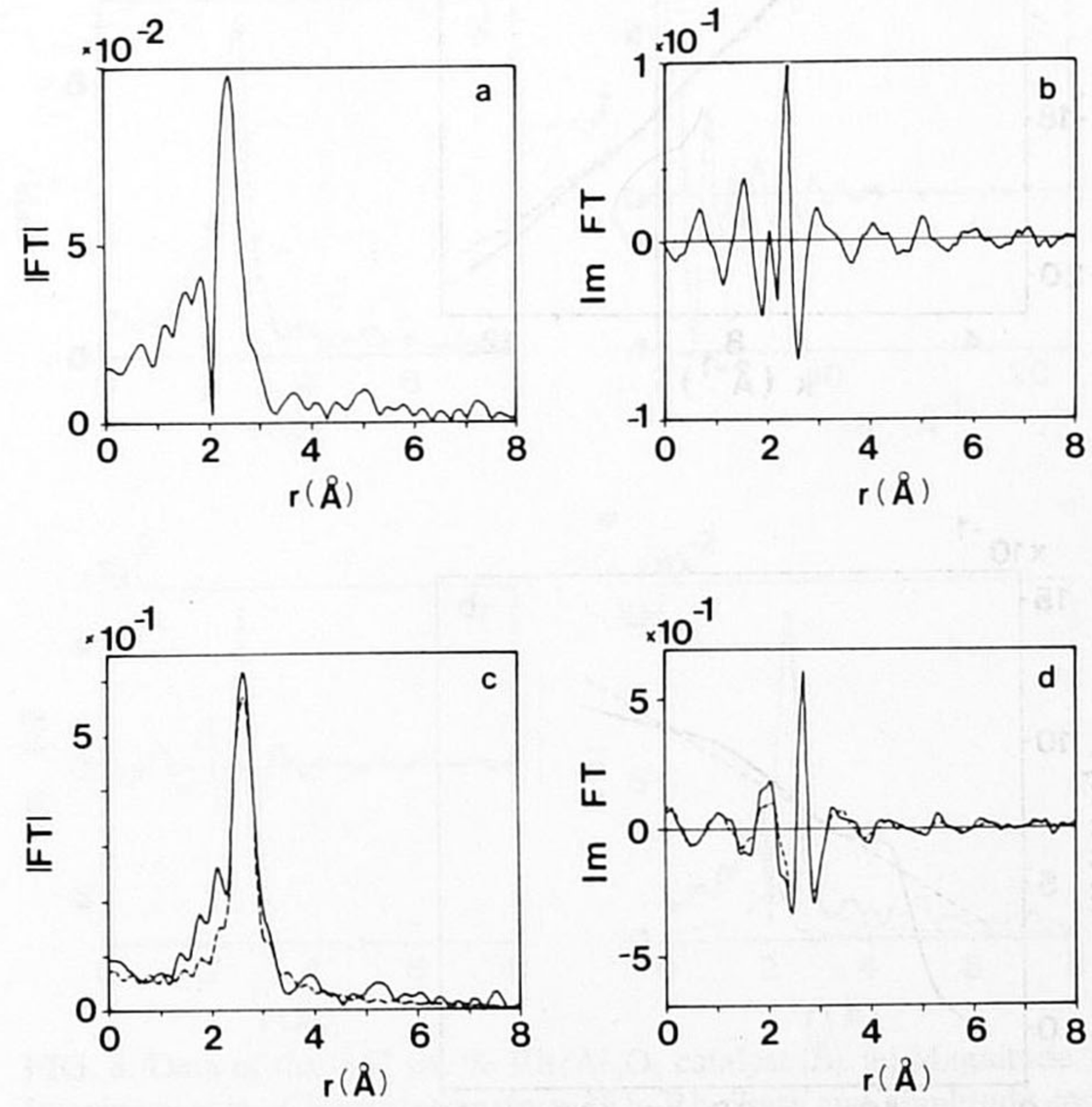

FIG. 5. Fourier transforms of the 0.47 wt. % Rh/Al_2O_3 catalyst (B) (k^1-weighed, $\Delta k = 3.3$–12.7 Å^{-1}). Normal: (a) magnitude, (b) imaginary part. Rh–Rh phase and amplitude corr.: (c) magnitude, (d) imaginary part. Solid line: experimental data, dotted line: calculated single Rh–Rh shell (see Table III).

Fourier transform is used. Figures 5(c) and 5(d) show the magnitude and the imaginary part of a k^{1}-weighed transform which is corrected for the rhodium–rhodium phase shift and backscattering amplitude (k min $= 3.3$ Å^{-1}, k max $= 12.7$ Å^{-1}). The lower limit of the transformation was chosen to be k min $= 3.3$ Å^{-1} to avoid truncation errors caused by the forward and inverse transforms of the reference data which are known to distort primarily both ends of the data set. The effects of the phase and amplitude correction on the Fourier transform can be seen from a comparison of Figs. 5(a) and 5(c). Due to the removal of the phase shift function, the position of the main peak is shifted towards the real rhodium–rhodium coordination distance, while due to the removal of the backscattering amplitude the peak on the low r side of the main peak has decreased in intensity. However, if this peak was only due to a single rhodium–rhodium shell, one would expect just a single symmetrical peak. Thus, the extra contributions which are still visible between $R = 1.2$ Å and $R = 2.4$ Å must be ascribed to the presence of other types of neighbor atoms.

A first estimate for the parameters of the mean peak at 2.7 Å was obtained by inverse transformation. Since it was presumed that the second, smaller peak was caused by a low-Z scatterer, containing only information at low k values, the inverse transformation was carried out after a k^{1}-weighted corrected Fourier transformation which emphasizes the Rh–Rh information. To extract the Rh–Rh information the inverse transformation was performed over an Δr interval, $\Delta r = 1.78$–3.06 Å. The initial parameter values for this single Rh–Rh shell were obtained by phase fitting [Eq. (5)] and the application of the log-ratio method [Eq. (6)] using the first Rh–Rh shell of Rh metal foil as the phase and amplitude reference. An EXAFS function was now calculated using these initial parameter values and the experimental phase and amplitude functions so that this function approximates the measured Rh–Rh EXAFS function. Subsequently, this calculated function was Fourier transformed and inverse transformed in exactly the same way as was done for the catalyst. This inverse transformed signal was then used as a reference signal in the phase fit and the log-ratio technique. Since the calculated EXAFS signal before transformation was close to the unknown measured signal, the reference signal contains almost the same transformation artefacts as the backtransformed unknown signal. Because phase fitting and the log-ratio technique are relative methods, the transformation artefacts are almost eliminated. Figures 6(a) and 6(b) show the results of the phase fit and the log-ratio plot, respectively. An optimal phase fit was obtained with $R = 2.664$ Å. The log ratio plot which showed some oscillations due to the contribution of oxygen and some oscillations due to the Fourier transform, resulted in a coordination number of $N = 4.9$ and a squared disorder parameter of $\Delta\sigma^2 = 0.0064$ Å^2. An EXAFS function has been calculated, using the obtained values and transformed in the same way as was done for the catalyst. Figures 5(c) and 5(d) compare the magnitude and the imaginary part of the corrected Fourier transforms performed on the catalyst data (solid line) and on the calculated Rh–Rh data using the refined values from above (dotted line). Differences between the two curves between $R = 1.2$ Å and $R = 2.4$ Å are clearly visible. In or-

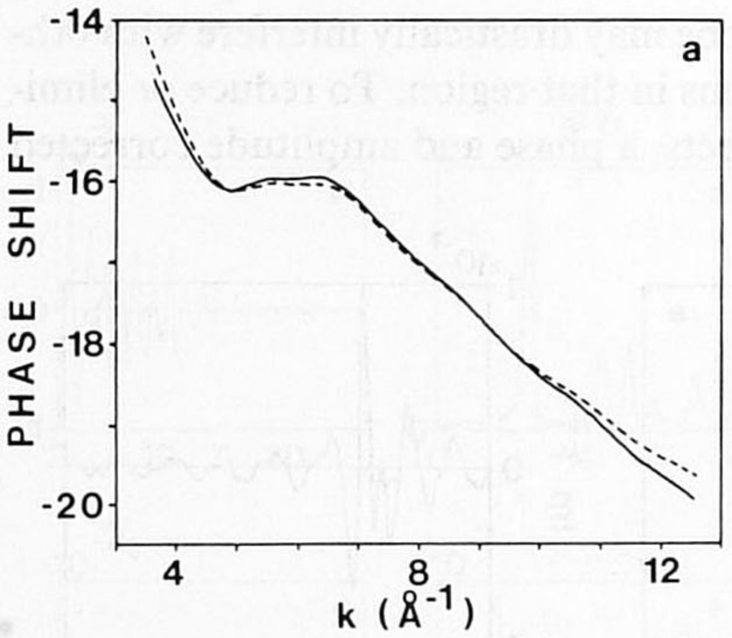

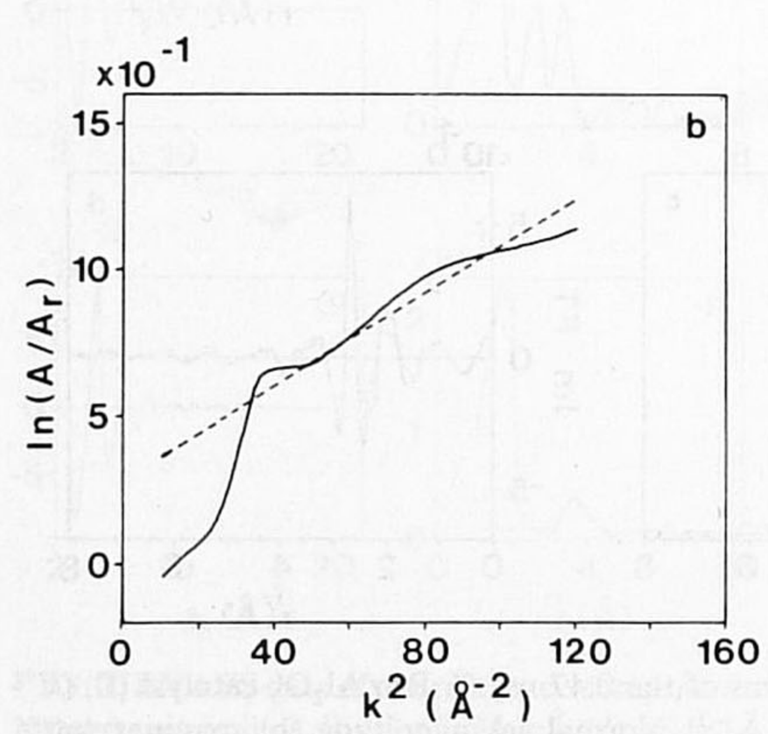

FIG. 6. (a) Phase shift function $\varphi(k)$ of the reference compound (dotted line) and catalyst (B) (solid line), (b) log plot of A/A_r vs k^2 (solid line). The dotted line represents the best fit straight line.

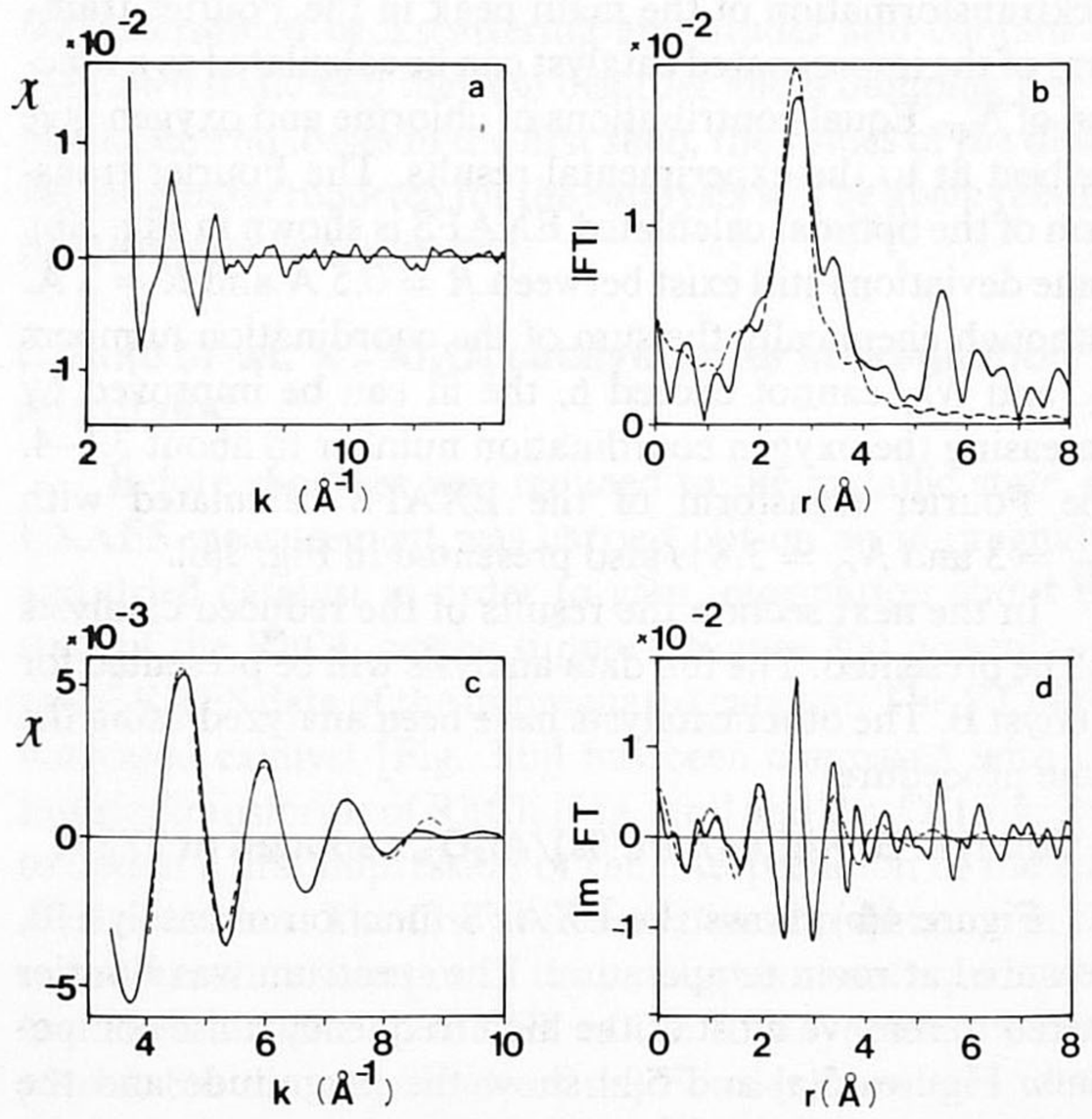

FIG. 7. Data of the 0.47 wt. % Rh/Al_2O_3 catalyst (B): (a) Difference spectrum obtained by subtracting the calculated Rh–Rh contribution from the experimental data. (b) Magnitude of the Fourier transform (k^{1}-weighed, Rh–O phase corrected, $\Delta k = 3.3$–10 Å^{-1}) of the difference spectrum and of the calculated Rh–O EXAFS (dotted line) (parameters see Table III). (c) Single shell EXAFS obtained after inverse transformation of (b) ($\Delta R = 1$–3.15 Å) (solid line) and best fit with Rh–O (dotted line). (d) Imaginary part of the Fourier transform as shown in (b).

der to analyze these differences and determine their origin, the calculated EXAFS function was subtracted from the measured signal of the catalyst, yielding the difference spectrum shown in Fig. 7(a). As a check on the chosen Rh–Rh parameters, the obtained residual spectrum has been Fourier transformed, corrected for the Rh–Rh phase shift. The absence of typical Rh–Rh beats around $R = 2.7$ Å in the imaginary part of the Fourier transform is an indication for the correctness of the Rh–Rh parameter values. Normally we find that these parameter values are already quite accurate. However, if no satisfactory difference spectrum is obtained, the parameter values can be optimized manually.

From the shape of the envelope in the difference spectrum, which is a monotonically decreasing function, it is concluded that the second scatterer must be a low-Z element. In this catalyst the most likely elements O and Cl have to be considered. A Fourier transformation, corrected for the Rh–O phase shift, was performed on the residual spectrum. Figures 7(b) and 7(d) (solid line) present the magnitude and the imaginary part of the k^{1}-weighted corrected Fourier transform, performed over an interval from $k = 3.4$ Å^{-1} to $k = 10$ Å^{-1}. Since Im FT′ peaks positively, the scatterer is identified as oxygen at a coordination distance of approximately 2.7 Å. Applying a Fourier transformation, corrected for Rh–Cl phase shift, did not result in a positively peaking imaginary part. A mixture of both O and Cl must also be excluded since the symmetry of the imaginary part strongly points to the presence of only one type of scatterer. The FT′ of the difference spectrum was inverse transformed over a range $\Delta r = 1.3$–3.1 Å. From the EXAFS oscillations which show the characteristics of an oxygen scatterer [Fig. 7(c), solid line], parameter values for this Rh–O contribution were obtained by a fit in k space from $k = 4$ Å^{-1} to $k = 9$ Å^{-1}. From the comparison between the backtransformed and best fit signal it is seen that a good fit was obtained [Fig. 7(c), dotted line]. An Rh–O EXAFS function was calculated from $k = 3.4$ Å^{-1} to $k = 10$ Å^{-1} with the best fit parameters (see Table III) and Fourier transformed (Rh–O phase corrected) [Figs. 7(b) and 7(d), dotted line]. Most of the features in the Im FT′ between $R = 0$ Å and $R = 3.2$ Å of the residual spectrum can be reproduced by the calculation.

TABLE III. Structural parameters for Rh^0–Rh^0 and Rh^0–O_s^{2-} coordination.

Catalyst	T (K)	Rh^0 - Rh^0			Rh^0 - O_s^{2-}		
		N	R (Å)	$\Delta\sigma^2 x10^3$ (Å^2)	N	R (Å)	$\Delta\sigma^2 x10^3$ (Å^2)
A	140	3.7	2.680	5.0	1.9	2.74	0
	300	3.8	2.667	6.6	-	-	-
B	95	5.3	2.680	5.1	1.3	2.73	0
	300	4.9	2.664	6.4	1.35	2.71	1
C	77	5.8	2.680	5.0	1.2	2.73	0
	300	5.7	2.670	6.8	1.2	2.68	1
D	90	6.5	2.687	3.2	1.0	2.73	0
	300	6.7	2.680	4.9	1.0	2.68	1

At this point a further check and if necessary a refinement of the Rh–Rh parameters can be obtained by subtracting the calculated Rh–O EXAFS signal from the measured EXAFS signal, resulting in a spectrum containing mainly a Rh–Rh signal. If the imaginary part of the Fourier transformation (k^{1}-weighed, Rh–Rh phase and amplitude corrected) of this difference spectrum is symmetric, then the Rh–Rh parameters which were used, are satisfactory. If it is not then an inverse transform of this spectrum can be reanalyzed for improved Rh–Rh parameter values. In this recursive way accurate parameter values can be obtained for both Rh–Rh and Rh–O. But in all cases, residual Fourier transforms containing only one type of scatterer, must show a symmetric imaginary part when the appropriate correction has been applied to the FT.

Finally, Figs. 8(a), 8(b), and 8(c) show, both in k space and r space, the experimental results of the catalyst (solid line) in comparison with the calculated EXAFS (dotted line), containing both Rh–Rh and Rh–O coordinations with optimized parameter values: $N_{Rh\text{–}O} = 1.3$, $R_{Rh\text{–}O} = 2.71$ Å, $\Delta\sigma^2 = 0.001$ Å^2. (See Table III.) The magnitude and the imaginary part of the Fourier transform are almost identical, giving confidence in the obtained results. Figure 8(d) shows separately the contributions of the Rh–Rh and the Rh–O distance in a normal Fourier transform. The Rh–O distance overlaps with the Rh–Rh distance, causing severe interference in the imaginary part. This clearly shows that one ought to be careful with a simple assignment of distances based on peak locations in the magnitude of the Fourier transform.

E. Catalyst A, (0.57 wt. %)Rh/Al_2O_3, reduced at 573 K

Figure 4(a) shows the EXAFS of this catalyst. The signal looks very similar to that of catalyst B, except for some

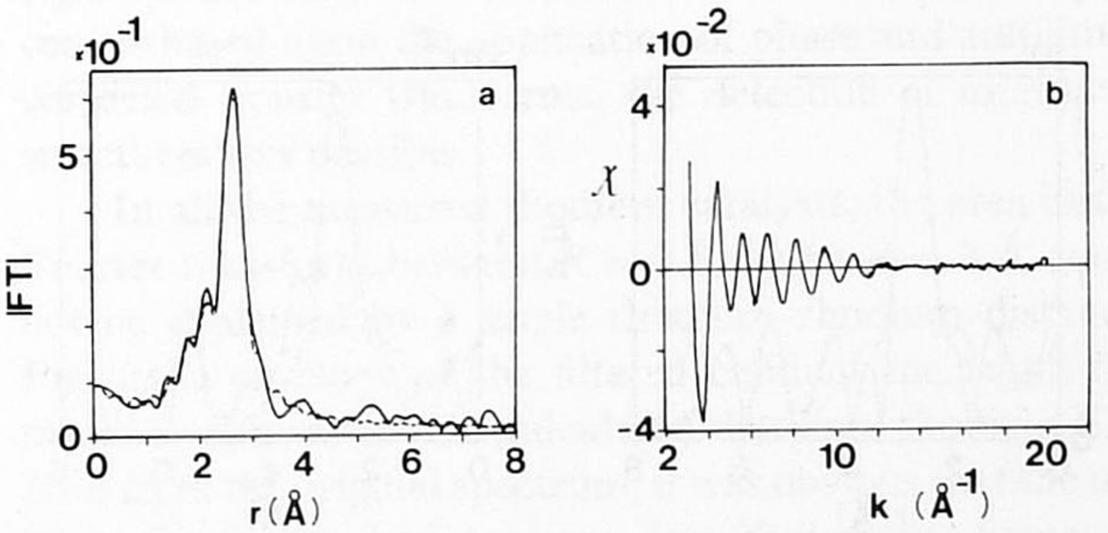

FIG. 8. Data of the 0.47 wt. % Rh/Al_2O_3 catalyst (B). (a) Magnitude. (c) Imaginary part of Fourier transform (Rh–Rh phase and amplitude corr., $\Delta k = 3.3$–12.7 Å^{-1}) of experimental data (solid line) and calculated Rh–Rh + Rh–O EXAFS (dotted line). (b) Experimental data (solid line) and calculated Rh–Rh + Rh–O EXAFS. (d) Magnitude of the Fourier transform (k^{1}-weighed, $\Delta k = 3.3$–12.7 Å^{-1}) of experimental data (solid line) and of calculated EXAFS: Rh–Rh (dotted line) and Rh–O (---).

differences around $k = 10$ Å^{-1}. We believe that the sharp dip at $k = 9$ Å^{-1} and the sudden decrease at $k = 10.5$ Å^{-1} is due to an artifact in the measurement and cannot be explained by any EXAFS simulation. Therefore, in this catalyst a maximum k value of 8.5 Å^{-1} was used to avoid the influence of the artifact. Using the same data analysis technique as applied to the 0.47 wt. % Rh/Al_2O_3 catalyst resulted in a Rh–Rh coordination number $N = 3.7$. This coordination number points to even smaller rhodium particles than present in catalyst B. The relatively larger contribution of the metal–support interface is confirmed by an increase in the measured Rh–O coordination number ($N_{Rh-O} = 1.9$). Figure 9(a) presents the Fourier transform of the residual spectrum, obtained after subtraction of the optimized Rh–Rh EXAFS function. The FT was corrected for Rh–O phase and again points to the presence of oxygen. Figure 10(a) shows the FT′ of the experimental data and the calculated EXAFS, containing the Rh–Rh and Rh–O coordination. Although the Rh–O distance is again 2.7 Å, a strong peak appeared now at a distance of 1.8 Å, due to interference between the Rh–Rh and Rh–O EXAFS functions.

F. Catalyst C, Rh(1.04 wt. %)/Al_2O_3, reduced at 773 K

The EXAFS function is shown in Fig. 4(c). Due to the larger rhodium loading as compared with catalyst B, the size of the metal particles is larger. However, due to the increased signal-to-noise ratio of the Rh–Rh EXAFS, the Rh–O contribution can still reasonably be detected. The corrected Fourier transform of the residual Rh–O signal is given in Fig. 9(c). The amplitude has decreased in comparison with the increase in particle size. Figure 10(c) shows the agreement between the FT′ of the measured signal and the calculated Rh–Rh and Rh–O EXAFS.

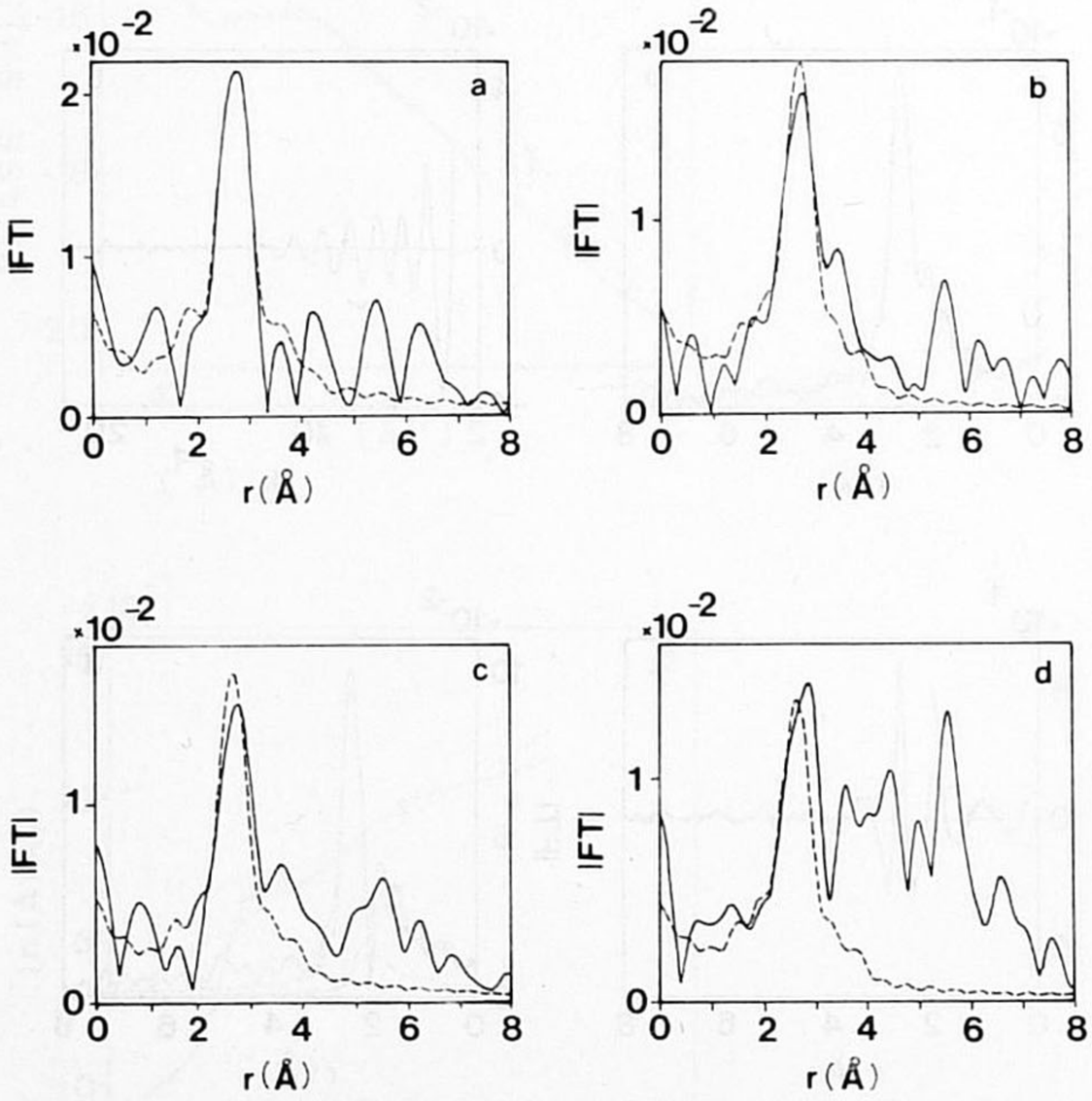

FIG. 9. Magnitude of the Fourier transform (k^1-weighed, Rh–O phase corrected) of the difference spectra, obtained after subtraction of the Rh–Rh contribution from the experimental data (solid line). The dotted line represents the transform of the calculated Rh–O signal. (a) 0.57 wt. % Rh/Al_2O_3, $\Delta k = 3.3$–8.5 Å^{-1}. (b) 0.47 wt. % Rh/Al_2O_3, $\Delta k = 3.3$–10 Å^{-1}. (c) 1.04 wt. % Rh/Al_2O_3, $\Delta k = 3.3$–10 Å^{-1}. (d) 2.00 wt. % Rh/Al_2O_3, $\Delta k = 3.3$–10 Å^{-1}.

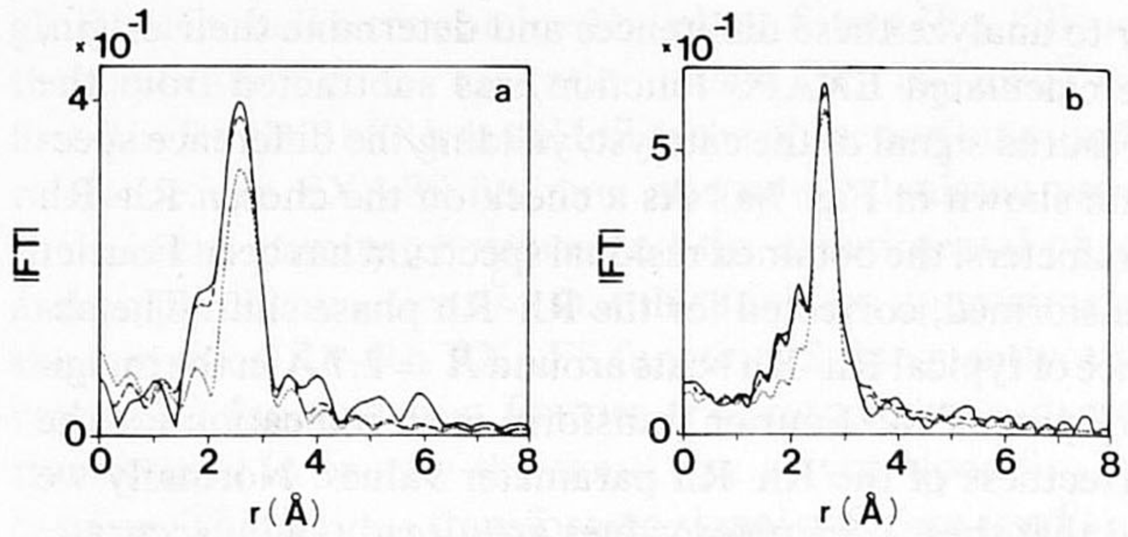

FIG. 10. Magnitude of the Fourier transform (k^1-weighed, Rh–Rh phase and amplitude corr.) of the catalyst (solid line), the calculated Rh–Rh (···) and Rh–Rh + Rh–O EXAFS (- - -). (a) Rh(0.57 wt. %)/Al_2O_3, $\Delta k = 3.3$–8.5 Å^{-1}. (b) Rh(0.47 wt. %)/Al_2O_3, $\Delta k = 3.3$–12.7 Å^{-1}. (c) Rh(1.04 wt. %)/Al_2O_3, $\Delta k = 3.3$–12.7 Å^{-1}. (d) Rh(2.00 wt. %)/Al_2O_3, $\Delta k = 3.3$–12.7 Å^{-1}.

G. Catalyst D, Rh(2.00 wt. %)/Al_2O_3, reduced at 573 K

The EXAFS function of the catalyst is given in Fig. 4(d). Again, the intensity of the signal has increased with respect to the previous catalysts. The particle size is further increased which is confirmed by the significant presence of higher coordination shells. Still, the main peak in the Fourier transform cannot be fully explained by a single rhodium–rhodium distance and a small amount of oxygen neighbors has to be included. Figures 9(d) and 10(d) give the FT′ of the calculated Rh–O and Rh–Rh + Rh–O EXAFS which closely correspond with the FT′ of the residual and the experimental spectrum, respectively. Despite the fact that the data extends to a maximum k value of 15 Å^{-1}, the FT was taken over the same interval as catalysts B and C to allow an easy comparison of the Fourier transforms.

The dotted lines in Fig. 10 represent the FT′ of the calculated Rh–Rh EXAFS functions demonstrating that the differences of these transforms with the transforms of the experimental data decrease with increasing particle sizes. The parameters of the Rh–Rh and Rh–O coordinations of catalysts A, B, C, and D are given in Table III. The relative accuracy of the Rh–Rh coordination number is estimated to be 10%, the coordination distance better than 1%. The value of the Rh–O distance is dependent on the value of the subtracted Rh–Rh distance, so the accuracy is estimated to be 2%–3%. The accuracy of N_{Rh-O} is dependent on the noise of the spectrum and the accuracy of the Rh–Rh coordination number, so the accuracy will be ~20%.

V. DISCUSSION

About equal contributions of oxygen and chlorine neighbors are present in the EXAFS of the impregnated and

dried catalyst. Yet, the Fourier transform of the impregnated catalyst is larger in the region $1 < R < 3$ Å than the FT of the calculation assuming a total coordination of six. At the same time the FT of the impregnated catalyst shows significant higher shell contributions between $R = 3$ Å and $R = 4$ Å. From these results, two models can be proposed for the initial state of the catalyst:

(i) Assuming that the rhodium is distributed homogeneously over the surface of the Al_2O_3 support, the equal coordination of chlorine and oxygen can be explained either by $Rh(H_2O)_3Cl_3$ complexes, deposited from solution which remain intact after drying, or by $Rh(O_s)_3Cl_3$ surface complexes formed by direct coordination to surface oxygen ions. Since the surface density of the rhodium ions is very low (~ 0.2 Rh/nm^2) the higher shell contributions, present between $R = 3$ Å and $R = 4$ Å, cannot be explained by interactions between different rhodium sites, if a homogeneous surface distribution is assumed. In this case the presence of higher shells must be ascribed to contributions of oxygen and/or aluminum ions from a second layer of the support.

(ii) It is also possible that, despite the low rhodium concentration, a mixture of isolated $Rh(H_2O)_3Cl_3$ surface complexes and small $RhCl_3$ agglomerates is formed. The higher shells can then be assigned to Rh–Rh distances and higher Rh–Cl distances in the agglomerates. Since such chloridic agglomerates will never contain more rhodium atoms than the metal particles which are generated from them, it follows from the analysis of the reduced catalyst that the agglomerates do not contain more than 10 rhodium ions.

The rhodium ions present on the surface of the γ-Al_2O_3 support as described above are converted into very small rhodium metal crystallites by reduction with H_2 at elevated temperatures. The measured average coordination numbers (3.7, 4.9, 5.7, and 6.7) of the four different catalysts are lower than coordination numbers reported in earlier papers for different metal supported catalysts.[1] Only Via *et al.*[4] claim a coordination number of 1.5 for a 0.5 wt. % Rh/Al_2O_3 catalyst.[4] However, the amplitude of their EXAFS signal is equal to the amplitude of our catalyst A ($N = 3.7$), which has a two times better signal-to-noise ratio. Therefore, it seems reasonable to believe that the coordination numbers of both catalysts are not too much different. The relative accuracy of the coordination numbers, determined with the data analysis described in this work, is estimated to be better than 10%. Therefore the increase in coordination number implies a significant increase in particle size. The same trend is noticeable in the hydrogen chemisorption experiments (see Table I).

The Debye–Waller factor (DWF) of the catalyst shows a significant deviation relative to the DWF of rhodium metal foil (measured at 77 K). A slightly decreasing DWF as function of increasing particle size can be noticed. As expected, the DWF measured at liquid nitrogen temperature is smaller than those measured at room temperature.

All highly dispersed rhodium catalysts show first shell coordination distances which are approximately equal to the first shell coordination distance in bulk rhodium (2.687 Å). This is in agreement with other results obtained on supported metal catalysts under the same experimental conditions. However, according to measurements of Apai *et al.*[22] on Ni and Cu supported on amorphous carbon, a contraction in the metal–metal bond length is expected to occur with decreasing particle size. Moraweck *et al.*[23] observed a contraction of 0.12 Å in the Pt–Pt coordination distance of platinum metal crystallites in a Y-zeolite catalyst when the catalyst was measured in vacuum, but they showed that the bond length relaxed to the bulk platinum distance (2.77 Å) after adsorption of hydrogen gas. In the latter case the platinum atoms at the surface of the particle are completely coordinatively saturated by the hydrogen, through which the bond length relaxes to the value in bulk platinum. A similar contraction was recently shown by van't Blik *et al.*[24] for a Rh/Al_2O_3 catalyst after evacuation. Since all our catalysts were measured under hydrogen, we expect to find no significant contraction in the bond length. The coordination distances which were measured at room temperature tend to be smaller than those measured for the liquid nitrogen spectra. This could be caused by the effect of an asymmetric distribution function.[16–18] Marques *et al.*[2] performed temperature dependent experiments on a 1 wt. % Pt/SiO_2 catalyst and determined the apparent contraction due to asymmetry at high temperatures. In the temperature region between 100 and 300 K they did not detect a contraction. However, this need not to be in contradiction with our measurements since their catalyst was less dispersed ($N = 7.5$) than ours.

As indicated by the hydrogen chemisorption measurements (Table I) and by the average coordination numbers (Table III), the size of the metal crystallites is very small. Therefore it is not surprising to see an interaction between the rhodium in the crystallites and the oxygen of the support, considering that for a very small crystallite a relatively large fraction of the rhodium atoms will be present in the interface layer between the particle and the support. Due to the good signal-to-noise ratio of the spectra and the data analysis procedure based upon the application of phase and amplitude corrected Fourier transforms, the detection of interfacial structures was possible.

In all the measured rhodium catalysts, the area in the Fourier transform between $R = 0.5$ Å and $R = 3$ Å could not be explained by a single rhodium–rhodium distance. From the envelope of the filtered residual spectrum, obtained by subtracting the calculated rhodium–rhodium EXAFS from the original spectrum, it was obvious that the unknown scatterer had to be a low-Z element. Since all catalysts were prepared by impregnating the oxidic γ-Al_2O_3 support with the precursor $RhCl_3 \cdot 3H_2O$, both the low-Z elements Cl and O had to be considered. The k dependence of the backscattering amplitude and the phase shift function of chlorine and oxygen are almost equal and can hardly be used to distinguish between the two scatterers. However, the phase function of oxygen shows a constant difference of approximately π radians with respect to the phase function of chlorine. The fact that apparently the EXAFS data of $RhCl_3$ [Fig. 2(g)] and Rh_2O_3 [Fig. 2(d)] are nearly in phase, is due to the difference in coordination distances. Therefore, only the phase of the imaginary part, obtained by a Rh–O phase shift corrected Fourier transform on the residual EXAFS spectrum, can be used to distinguish between the two possible scatterers. The results showed that the low-Z element for all

of the reduced catalysts was oxygen. There are three possible origins for this oxygen:

(i) The catalyst was not completely reduced. However, TPR measurements showed that more than 95% of the catalyst was reduced.[10] Besides, an incompletely reduced catalyst would show oxidic distances (~2.05 Å) for the rhodium–oxygen bond[25] instead of the measured Rh–O coordination distance of 2.7 Å.

(ii) The oxygen could be caused by contamination with air during the treatment. This would have led to an incomplete reduction of the very small metallic particles, which again would have been detected as an oxidic distance of 2.05 Å.

(iii) Oxygen could come from the support so that the observed Rh–O bond represents the interaction of the metal crystallite with the surface layer of the support.

The measured Rh–O coordination distance of 2.7 Å is almost 0.7 Å larger than the oxidic Rh–O distance such as in Rh_2O_3 (2.05 Å). Considering that the radius of an Rh^{3+} ion, such as present in Rh_2O_3, is about 0.7 Å smaller than the radius of the Rh atoms in the metal crystallites, a bond length of 2.7 Å can be explained by an interaction between zero valent Rh atoms and oxygen ions of the support. For catalytic systems such as Ni/SiO_2, Ni/Al_2O_3, and Co/Al_2O_3[26–29] it is well known that the metal particle is bound to the support via an interdiffusion of the metal oxide and the oxidic support. However, for Rh and Pt supported catalysts, the mechanism of the metal–support interaction is still unknown. Koningsberger *et al.*[25] have recently shown that for Rh/Al_2O_3 catalysts the binding of the metallic rhodium particle with the oxidic support is not caused by an oxidic layer with normal cation (Rh^{3+})–anion (O^{2-}) distances. The measured long Rh–O coordination distance of 2.7 Å is a strong indication that the binding of the metallic rhodium particle with the oxidic support takes place by an ion-induced dipole interaction between the support oxygen ions and the metal atoms present in the interface between metal particle and support. This kind of bonding mechanism was already proposed by our group for a 0.5 wt. % Rh/Al_2O_3 catalyst.[5] The results presented in this work are a further confirmation of this kind of interaction.

Questions may arise about the use of the Rh^{3+}–O^{2-} absorber scatterer pair as a reference compound for the determination of the Rh^0–O_s^{2-} parameters. Besides the backscattering amplitude and Debye–Waller factor, the EXAFS amplitude is also determined by the atomic overlap factor (S_0^2) and the mean free path (λ).[13] A nontransferability of one of these parameters causes a wrong determination of the Rh^0–O_s^{2-} coordination number. According to Stern, the EXAFS is only affected by the atomic values of S_0^2 and not by chemical variations of the absorber. Therefore, a change in the valence state of the central atom ($Rh^{3+} \rightarrow Rh^0$) will hardly have any influence on the amplitude. His results also show that, despite the dependence of λ and Δ with the ionicity of the bond, for the first coordination shell the exponential term is equal to 1 within the limits of accuracy. So, in the ideal case no correction has to be made to the determined Rh^0–O_s^{2-} coordination number. The fact that both systems are reasonably identical is supported by the small differences in the measured phase shift functions. On the other hand, the central rhodium atom is also surrounded by other rhodium metal atoms. If the Rh^0–O_s^{2-} distance is treated as a second shell, a correction of 20%–30% should be made due to the different coordination distances of the Rh^{3+}–O^{2-} and the Rh^0–O_s^{2-} bond. In this case the determined coordination numbers will be too low. Since it is very difficult to obtain a suitable reference compound for the Rh^0–O_s^{2-} bond, no accurate coordination number can be given, but following the above considerations the measured coordination number will be 0%–30% too low.

By comparing the measured average Rh–Rh and Rh–O coordination numbers with model calculations, it is possible to obtain information about the structure of the metal–support interface. The Rh–Rh coordination numbers obtained for the first shell are directly correlated with the size and shape of the metal particle. Assuming a certain particle shape and structure, one can theoretically calculate the expected average first shell Rh–Rh coordination number as a function of the particle diameter.

We will use a simple model to gain insight into possible interfacial structures. Since our knowledge about the morphology of the rhodium particles is not complete, this model is not intended as a specific proposal for the structure of these particles. Nevertheless we feel that it does give an idea about some of the aspects of the structure of the interface between particles and support. In Fig. 11 we show the result of our calculation for the Rh–Rh coordination number vs particle diameter for rhodium particles having an fcc structure and an approximately half spherical shape. These calculations were done by successively adding more and more atoms to the particle while keeping the fcc way of packing and approaching as much as possible the half spherical shape. The jumps in the curve are due to the discrete growth of the particle. The total number of atoms in a half spherical particle, N_t, can now be derived from the equation:

$$N_t = f_p\, V_p / V_a = f_p\, d^3/(16\, R_{at}^3), \tag{8}$$

where V_p is the volume of the particle, V_a the volume of a rhodium atom, f_p the packing fraction, d the diameter of the particle, and R_{at} the radius of a rhodium atom. For smaller diameters there may be some deviation from this simple model. The number of atoms, N_{int}, which are in a half-spherical shape present at the interface between particle and support, can be calculated in the same way, resulting in

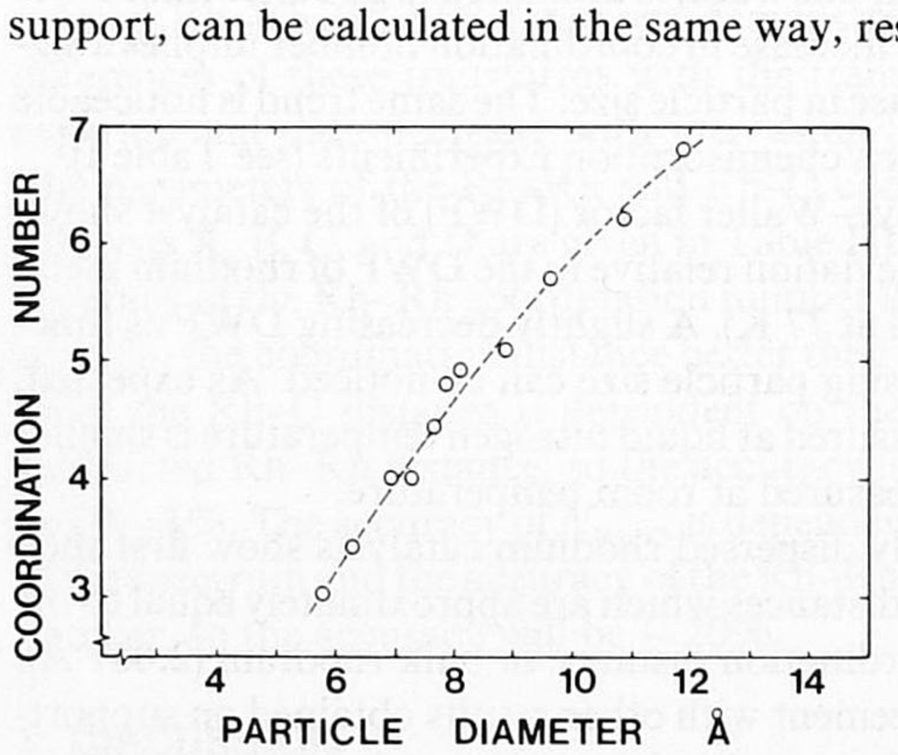

FIG. 11. First shell Rh–Rh coordination number as a function of the diameter of a half-spherical rhodium particle, having an fcc structure.

$$N_{\text{int}} = f_p\, d^{\,2}/(4R^{\,2}_{at}). \quad (9)$$

Since the measured oxygen coordination number of a rhodium atom, $N_m(Rh^0\text{–}O_s^{2-})$, is an average over all rhodium atoms, the coordination number, $N_c(Rh^0\text{–}O_s^{2-})$, which represents the real number of oxygen ions, which are in contact with a rhodium atom in the metal–support interface, can be derived from the equation:

$$N_c(Rh^0\text{–}O_s^{2-}) = N_m(Rh^0\text{–}O_s^{2-})d\,/(4R_{at}). \quad (10)$$

Table IV summarizes the expected particle diameter, average number of rhodium atoms per particle, the number of interfacial rhodium atoms, and the measured Rh–O coordination numbers for the four catalysts. Figure 12 shows the measured Rh–O coordination number as a function of the measured Rh–Rh coordination number. Using Eq. (10) and the relation between the particle diameter and the measured Rh–Rh coordination number (Fig. 11), it is now possible to calculate the average number of oxygen atoms which are coordinated to the interfacial rhodium. In Fig. 12 we have drawn three lines for $N_c = 2$, 3, and 4. It is clear that within the uncertainty of the measurements all our catalysts confirm the values $2 < N < 3$.

Based on these results we can now make some general remarks about the structure of the metal–support interface of our catalysts.

The γ-alumina support is a complicated surface which may consist of a mixture of low index surface planes such as (111), (110), and (100) planes.[30] All exposed faces might serve as sites for metallic rhodium particles. The coordination of rhodium with oxygen will depend on the structure of the surface plane and the structure of the rhodium particle. Rhodium particles were modeled based on the assumption of an epitaxial growth onto the surface support, which is quite possible since there is only a slight difference between the oxygen–oxygen distance of the support (2.80 Å) and the rhodium–rhodium distance in the metal crystallite (2.687 Å). For each of the planes which were considered, two sites were found possible, as shown in Fig. 13. One type of site is energetically less favorable and gives for each plane an oxygen coordination of 2 for every rhodium atom in the interface. The energetically more favorable sites have interfacial rhodium atoms coordinated by 4, 4 and 3 oxygen ions for the (100), (110), and (111) planes, respectively. The Rh–O coordination number of 2–3 can thus be explained by rhodium particles which are situated on a variety of (110), (111), and (100) planes of the alumina or by rhodium particles which are epitaxially grown on an Al_2O_3 (111) surface. It is also possible that rhodium particles grow onto all kinds of defects, kinks, and steps present on the γ-Al_2O_3 surface, resulting in an average oxygen coordination of 3. It should be stressed that the above results have been obtained under the assumption of half spherical fcc rhodium particles which grow epitaxially on ideal low index surface planes of γ-Al_2O_3. Another approach could have been to model the rhodium particles under the assumption of nonideal γ-Al_2O_3 surface planes. Since the rhodium was reduced to temperatures of at least 573 K, one might envisage that some dehydroxylation of the support surface has taken place.[30] The $Rh^0\text{–}O_s^{2-}$ bond distances in the interface are consistent with those for unprotonated O^{2-} ions in the interfacial region. One can also fit in that case the measured N(Rh–Rh) and

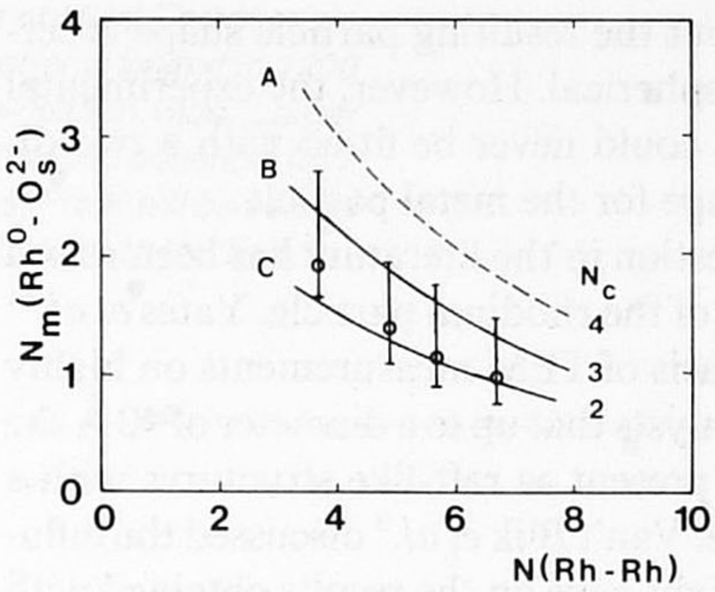

FIG. 12. $N_m(Rh^0\text{–}O_s^{2-})$ coordination number vs the measured Rh–Rh coordination number. The dots represent measured values with limits of accuracy and 30% uncertainty (see the text). The lines indicated by A, B, and C reflect Eq. (10) with $N_c(Rh^0\text{–}O_s^{2-})$ 4, 3, and 2, respectively.

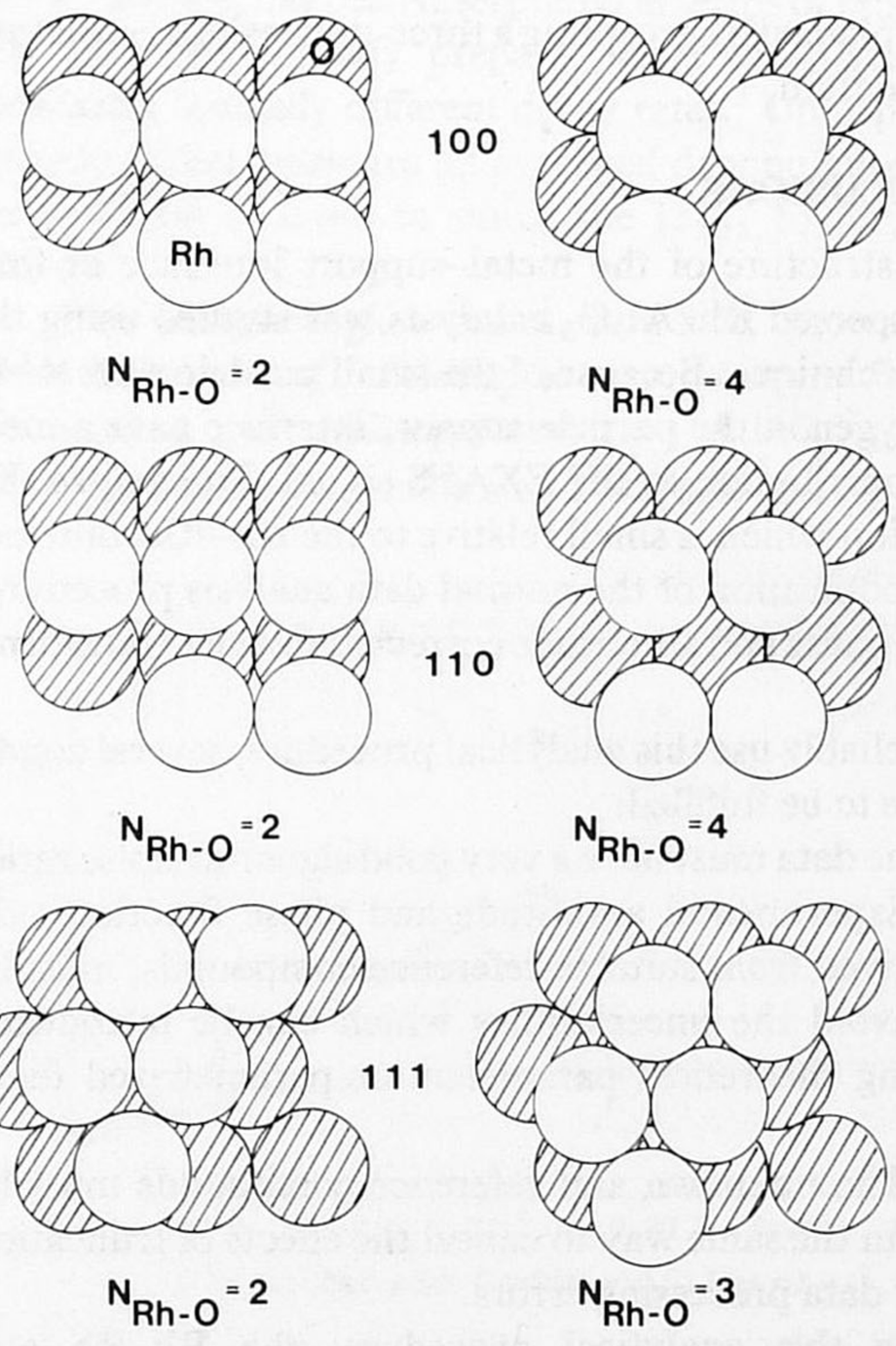

FIG. 13. First layer of the rhodium particle positioned onto several γ-Al_2O_3 surface sites (100, 110, and 111 faces). The average Rh–O coordination number, $N_{Rh\text{–}O}$, depends on the surface structure of the alumina and the position of the rhodium particle.

TABLE IV. Relation between particle size, number of atoms, and measured coordination numbers.

N(Rh-Rh)	d (Å)	Number of atoms	Number of interfacial atoms	$N_m(Rh^0\text{-}O_s^{2-})$
3.7	6.7	7	5	1.9
4.9	8.4	12	7 - 8	1.35
5.7	10	20	11	1.2
6.7	12	35	15 - 16	1.0

$N(Rh^0–O_s^{2-})$ values, but the resulting particle shape is certainly not always half spherical. However, the experimental coordination numbers could never be fitted with a two-dimensional raft-like shape for the metal particle.

An important question in the literature has been raised about the morphology of the rhodium particle. Yates *et al.*[31] have asserted on the basis of TEM measurements on highly dispersed rhodium catalysts that up to a diameter of 40 Å the rhodium particles are present as raft-like structures with a two-dimensional shape. Van't Blik *et al.*[3] discussed the influence, which oxygen might have on the results obtained with TEM measurements. They concluded that rhodium is present as three-dimensional crystallites. There are several arguments to reject the idea of two-dimensional structures. (i) Catalyst B shows a Rh–Rh coordination number of 4.9 which, assuming one atom thick two-dimensional (111) rafts, implies a particle which has a diameter of 40 Å and contains about 200 atoms of which 50 atoms belong to the edges and corners of the particle. Taking an H/Rh stoichiometry of 2 for the edge and corner atoms and 1 for the "interior" atoms[31] hydrogen chemisorption experiments would have resulted in an H/Rh value of 1.2 instead of the measured value of 1.7. (ii) The measured average oxygen coordination number (N_m) of the rhodium decreases with increasing particle size in accordance with a three-dimensional structure, while in the case of a two-dimensional raft the coordination number would be independent of the particle size. The measured coordination numbers of one catalyst alone cannot distinguish between a two-dimensional or a three-dimensional structure. The EXAFS results of all four catalyst and the hydrogen chemisorption measurements can only be explained by accepting a three-dimensional structure for the rhodium.

VI. CONCLUSIONS

The structure of the metal–support interface of four highly dispersed Rh/Al_2O_3 catalysts was studied using the EXAFS technique. Because of the small particle sizes (6–12 Å) the oxygen at the particle support interface gave a measurable contribution to the EXAFS signal. To analyze this contribution which is small relative to the Rh–Rh contribution, a modification of the normal data analysis procedures involving phase and amplitude corrected Fourier transforms was used.

To reliably use this analytical procedure, several conditions have to be fulfilled:

(i) The data must have a very good signal-to-noise ratio.

(ii) Experimental amplitude and phase functions, directly derived from suitable reference compounds, must be used to avoid the uncertainties which can be introduced when using theoretical parameters or parametrized functions.

(iii) The unknown and reference compounds must be analyzed in the same way to cancel the effects of truncation and other data processing errors.

Using this analytical procedure, the Rh–Rh and $Rh^0–O_s^{2-}$ coordination numbers were found for each catalyst. From these results the average number of oxygen ions in contact with an interfacial rhodium atom was determined to be 2–3, while the corresponding $Rh^0–O_s^{2-}$ bond length was 2.7 Å. This bond length strongly indicates that in the Rh/Al_2O_3 system the metal–support interaction is between zero valent Rh atoms at the interface and oxygen ions of the support.

ACKNOWLEDGMENTS

This work was done at SSRL (Stanford University, U. S. A.) which is supported by the Department of Energy, the National Science Foundation, and the National Institutes of Health. The authors gratefully acknowledge the assistance of the SSRL staff and the assistance of Dr. T. Huizinga in the preparation and measurements of some of the catalysts. The authors are indebted to Professor R. Prins for his encouragement and critical reading of the manuscript. This study was supported by the Netherlands Foundation for Chemical Research (SON) with financial aid from the Netherlands Organization for the Advancement of Pure Research (ZWO). One of us (DCK) would like to thank ZWO also for supplying a travel grant (R71-24).

[1]G. H. Via, J. H. Sinfelt, and F. W. Lytle, J. Chem. Phys. **71**, 690 (1979).
[2]E. C. Marques, D. R. Sandstrom, F. W. Lytle, and R. B. Greegor, J. Chem. Phys. **77**, 1027 (1982).
[3]H. F. J. van't Blik, J. B. A. D. van Zon, T. Huizinga, J. C. Vis, D. C. Koningsberger, and R. Prins, J. Phys. Chem. **87**, 2264 (1983).
[4]G. H. Via, G. Meitzner, F. W. Lytle, and J. H. Sinfelt, J. Chem. Phys. **79**, 1527 (1983).
[5]J. B. A. D. van Zon, D. C. Koningsberger, H. F. J. van't Blik, R. Prins, and D. E. Sayers, J. Chem. Phys. **80**, 3914 (1984).
[6]I. W. Bassi, F. W. Lytle, and G. Parravano, J. Catal. **42**, 139 (1976).
[7]G. Cocco, S. Enzom, G. Fagherazzi, L. Schiffini, I. W. Bassi, G. Vlaic, S. Galvano, and G. Parravano, J. Phys. Chem. **83**, 2527 (1979).
[8]F. W. Lytle, G. H. Via, and J. H. Sinfelt, J. Chem. Phys. **67**, 3831 (1977).
[9]P. Lagarde, T. Murata, G. Vlaic, E. Freund, H. Dexpert, and J. P. Bournonville, J. Catal. **84**, 333 (1983).
[10]J. C. Vis, H. F. J. van't Blik, T. Huizinga, J. van Grondelle, and R. Prins, J. Mol. Catal. **25**, 367 (1984).
[11]D. C. Koningsberger and J. W. Cook, in *EXAFS and Near Edge Structures*, edited by A. Bianconi, L. Incoccia, and S. Stipcich (Springer, Berlin, 1983), p. 412.
[12]J. W. Cook, Jr. and D. E. Sayers, J. Appl. Phys. **52**, 5024 (1982).
[13]E. A. Stern, B. A. Bunker, and S. M. Heald, Phys. Rev. B **21**, 5521 (1980).
[14]E. A. Stern, Phys. Rev. B **10**, 3027 (1974).
[15]F. W. Lytle, D. E. Sayers, and E. A. Stern, Phys. Rev. B **11**, 4825 (1975).
[16]P. Eisenberger and G. S. Brown, Solid State Commun. **29**, 481 (1979).
[17]E. D. Crozier and A. J. Seary, Can. J. Phys. **58**, 1388 (1980).
[18]E. D. Crozier and A. J. Seary, Can. J. Phys. **59**, 876 (1981).
[19]C. Bouldin and E. A. Stern, Phys. Rev. B **25**, 3462 (1982).
[20]E. A. Stern, D. E. Sayers, and F. W. Lytle, Phys. Rev. B **11**, 4836 (1975).
[21]P. A. Lee and G. Beni, Phys. Rev. B **15**, 2862 (1977).
[22]G. Apai, J. F. Hamilton, J. Stohr, and A. Thompson, Phys. Rev. Lett. **43**, 165 (1979).
[23]B. Moraweck, G. Clugnet, and A. J. Renouprez, Surf. Sci. **81**, L631 (1979).
[24]H. F. J. van't Blik, J. B. A. D. van Zon, D. C. Koningsberger, and R. Prins, J. Mol. Catal. **25**, 379 (1984).
[25]D. C. Koningsberger, J. B. A. D. van Zon, H. F. J. van't Blik, G. J. Visser, R. Prins, A. N. Mansour, D. E. Sayers, D. R. Short, and J. R. Katzer, J. Phys. Chem. (submitted).
[26]H. Suzuki, S. Takasaki, I. Koga, A. Meno, Y. Kotera, T. Sato, and N. Tode, Chem. Lett. 127 (1982).
[27]E. G. Derouane, A. J. Simoens, and J. C. Vedrine, Chem. Phys. Lett. **52**, 549 (1977).
[28]R. B. Shalvoy, B. H. Davis, and P. J. Rencroft, Surf. Int. Anal. **2**, 11 (1980).
[29]R. B. Greegor, F. W. Lytle, R. L. Chin, and D. M. Hercules, J. Phys. Chem. **85**, 1232 (1981).
[30]H. Knozinger and P. Ratnasamy, Catal. Rev. Sci. Eng. **17**, 31 (1978).
[31]D. C. Yates, L. L. Murrell, and E. B. Prestridge, J. Catal. **57**, 41 (1979).